ARCHIVES OF ELECTRICAL ENGINEERING VOL. 72(4), pp. 1035–1053 (2023)

DOI 10.24425/aee.2023.147425

A fault location method for hybrid transmission lines based on empirical Fourier decomposition

CAIXIA TAO, BAOSHENG XING ✉, TAIGUO LI

School of Automation and Electrical Engineering, Lanzhou Jiaotong University
Gansu Province, China
e-mail: {1733425004/✉1057597913/418832140}@qq.com

(Received: 12.07.2023, revised: 02.09.2023)

Abstract: This paper aims to address the problems of inaccurate location and large computation in hybrid transmission line traveling wave detection methods. In this paper, a new fault location method based on empirical Fourier decomposition (EFD) and the Teager energy operator (TEO) is proposed. Firstly, the combination of EFD and the TEO is used to detect the time difference between the arrival of the initial traveling wave of the fault at the two measurement ends of the hybrid line. Then, when the fault occurs at the midpoint of each line segment and at the connection point of the hybrid line, the time difference between the arrival of the fault traveling wave at the two measurement ends of the line is calculated according to the line parameters. By comparing the obtained time differences, it is determined whether the fault occurs in the first or second half of the line. Finally, the fault distance is calculated using the double-ended traveling wave method according to the fault section. The model was built on PSCAD and the proposed algorithm was simulated on MATLAB platform. The results demonstrate that the proposed method achieves an average fault location accuracy of 98.88% by adjusting transition resistances and fault distances and comparing with other location methods. After validation, the proposed method for locating faults has a high level of accuracy in location, computational efficiency, and reliability. It can accurately identify fault segments and locations in hybrid transmission line systems.

Key words: empirical Fourier decomposition, fault location, hybrid lines, Teager energy operator, traveling wave method

1. Introduction

In order to maintain a clean and beautiful city and better utilize land space, the number of overhead lines inside the city continues to decrease, while underground cables gradually increase. The original structure of the distribution network, consisting solely of overhead lines, has gradually transformed into a hybrid system incorporating both cables and overhead lines [1, 2]. Due to the

underground use of cables, the failure rate is relatively low compared to overhead lines. However, with the increase in usage time, cables may also fail due to insulation aging. Whether it is an overhead line or a cable line fault, if not dealt with in a timely manner, it may cause serious economic losses. Therefore, it is important to locate the fault location quickly and accurately after a fault occurs in a hybrid line to improve the reliability of power supply and reduce the loss of power outage [3, 4].

Currently, many studies have been conducted based on single overhead lines or cable lines. Due to the inconsistent characteristic impedance of hybrid lines, the traditional method of locating faults on a single type of line will no longer be applicable. The fault location methods for hybrid lines are mainly divided into two categories, namely impedance method [5] and traveling wave method [6]. The impedance method has the advantages of economy and simplicity in fault location of underground cables and overhead transmission lines [7], but its positioning results are greatly influenced by factors such as system operation, line impedance, and load current. The traveling wave method has better application value compared to the impedance method [8, 9], which can be divided into single ended method [10] and double ended method [11, 12]. The key step is to accurately detect the traveling wave head [13, 14]. Xie *et al*. [15] identified fault zones by defining and comparing the node ratio coefficient values of nodes and fault points based on the refractive characteristics of traveling waves at nodes, and proposed a hybrid line fault location method based on extreme-point symmetric mode decomposition (ESMD) combined with the Teager energy operator (TEO). This method has good reliability in fault line segment identification and eliminates the impact of changes in traveling wave velocity on hybrid line fault location, However, this method does not reflect the computational efficiency of ESMD for fault traveling wave signals. Duan *et al*. [16] proposed the use of ensemble empirical mode decomposition (EEMD) combined with symmetric differential energy operator (SDEO) to analyze fault traveling wave signals in the empirical mode decomposition (EMD) method, which is difficult to extract fault information due to the significant impact of mixed mode problems on the decomposed modal components. However, this method may lead to excessive computational complexity. Gashteroodkhani *et al*. [17] used the extracted transient voltage signal information to train a support vector machine, which was used to identify fault segments and locate the precise location of faults through the Bewley plot and transformed voltage signals. However, different fault conditions require different training of the support vector machine, so this method requires a large amount of data for training.

In this paper, a fault location method based on the empirical Fourier decomposition (EFD)-TEO is proposed for the problems of inaccurate location and high computational complexity in hybrid transmission line travelling wave detection methods. Furthermore, we propose a fault interval judgment method that utilizes the midpoints of each line segment and the connection points of hybrid lines. The simulation results show that the hybrid line fault location method proposed in this paper has high positioning accuracy, computational efficiency, and good reliability, which is more conducive to rapid and accurate fault location.

2. Fault traveling wave head detection method based on EFD-TEO

2.1. Traveling wave phase-mode transformation

Due to the coupling phenomenon between the three-phase lines, in order to better analyze the traveling wave signals, the Karrenbauer transform is used to decouple the current traveling wave

signals. According to the Karrenbauer transform, the transient traveling wave can be decomposed into the zero-mode component and the aerial mode component [18], and its expression is as follows:

$$\begin{bmatrix} \dot{I}_0 \\ \dot{I}_\alpha \\ \dot{I}_\beta \end{bmatrix} = \frac{1}{3} \begin{bmatrix} 1 & 1 & 1 \\ 1 & -1 & 0 \\ 1 & 0 & -1 \end{bmatrix} \begin{bmatrix} \dot{I}_A \\ \dot{I}_B \\ \dot{I}_C \end{bmatrix}, \tag{1}$$

where: $\dot{I}_\alpha$ and $\dot{I}_\beta$ are the aerial mode components, $\dot{I}_0$ is the zero-mode component; $\dot{I}_A$, $\dot{I}_B$, and $\dot{I}_C$ are the A, B, and C phase currents of the fault line, respectively.

Due to the severe attenuation of the zero-mode component, the aerial-mode component $\dot{I}_\alpha$ is used for the analysis in this paper.

2.2. Principle of empirical Fourier decomposition

EFD is an accurate adaptive signal decomposition method that has higher decomposition accuracy and computational efficiency for complex nonlinear and non-stationary signals [19]. EFD consists of two key steps: an improved segmentation technique and the construction of a zero-phase filter bank. This segmentation technique solves the problem of inconsistent decomposition results in the Fourier decomposition method (FDM) [20]. The use of zero phase filter banks further solves the problem of modal aliasing in EFD based on the empirical wavelet transform (EWT) [21], promoting accurate decomposition of the original signal.

2.2.1. Improved segmentation techniques

In the segmentation technique, $[0, \pi]$ is divided into adjacent frequency bands, and the values of ω_0 and ω_n are determined during the adaptive sorting process. During the sorting process, the Fourier spectrum amplitudes and their local maxima at $\omega = 0$ and $\omega = \pi$ were determined. The frequencies corresponding to the first N maxima in the sorting sequence were represented by $[\Omega_1, \Omega_2, \ldots, \Omega_N]$, $\Omega_0 = 0$ and $\Omega_{N+1} = \pi$ were defined. The boundary of each segment is represented by Eq. (2):

$$\omega_n = \begin{cases} \arg\min X_n(\omega) & \text{if } 0 \le n \le N,\ \Omega_n \ne \Omega_{n+1} \\ \Omega_n & \text{if } 0 \le n \le N,\ \Omega_n = \Omega_{n+1} \end{cases}, \tag{2}$$

where $X_n(\omega)$ is the Fourier spectrum amplitude between Ω_n and Ω_{n+1}.

2.2.2. Construction of zero-phase filter banks

In each frequency band, a zero-phase filter is a bandpass filter with cutoff frequencies ω_n and ω_{n-1}, and there is no transition phase. Therefore, the zero-phase filter retains the main Fourier spectral components within the segment, while excluding all other Fourier spectral components outside the segment. The zero-phase filter bank is shown in Fig. 1.

The Fourier transform of the signal $f(t)$ to be decomposed is represented as:

$$\hat{f}(\omega) = \int_{-\infty}^{\infty} f(t) e^{-j\omega t}\, \mathrm{d}t. \tag{3}$$

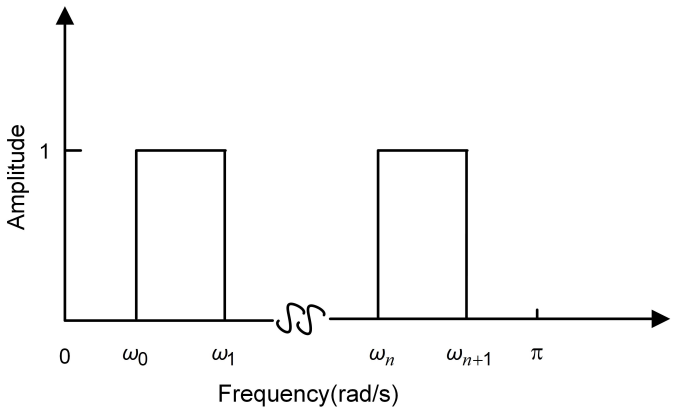

Fig. 1. EFD ideal filter bank

The zero-phase filter bank can be represented as:

$$\hat{\mu}_n(\omega) = \begin{cases} 1 & \text{if } \omega_{n-1} \le |\omega| \le \omega_n \\ 0 & \text{otherwise} \end{cases}, \tag{4}$$

where the values of $1 \le n \le N$ and ω_n are determined by Eq. (2).

The filtered signal corresponding to $\hat{\mu}_n(\omega)$ is represented as:

$$\hat{f}_n(\omega)j = \hat{\mu}_n(\omega)\hat{f}(\omega) = \begin{cases} \hat{f}(\omega) & \text{if } \omega_{n-1} \le |\omega| \le \omega_n \\ 0 & \text{otherwise} \end{cases}. \tag{5}$$

The decomposed components in the time domain can be obtained through inverse Fourier transform:

$$f_n(t) = \int_{-\omega_n}^{-\omega_{n-1}} \hat{f}(\omega)e^{j\omega t}\,\mathrm{d}\omega + \int_{\omega_{n-1}}^{\omega_n} \hat{f}(\omega)e^{j\omega t}\,\mathrm{d}\omega. \tag{6}$$

The reconstructed signal is calculated as the sum of all decomposed components:

$$\widetilde{f}(t) = \sum_{n=1}^{N} f_n(t). \tag{7}$$

2.3. Teager energy operator

The Teager energy operator is a signal analysis algorithm that can quickly and accurately calculate the instantaneous energy of a signal, with the advantages of low computational complexity and high temporal resolution [22].

The energy operator of continuous signal $s(t)$ is defined as:

$$\psi[s(t)] = s'^2(t) - s(t)s'', \tag{8}$$

where $s'(t)$ and s'' are the first and second derivative of $s(t)$.

The energy operator of discrete signals $s(n)$ is defined as:

$$\psi[s(n)] = s^2(n) - s(n+1)s(n-1). \tag{9}$$

When a fault occurs in a transmission line, the traveling wave undergoes an energy mutation during the transmission of the line. In this paper, the TEO is used to detect the energy mutation point. Therefore, the combination of EFD and the TEO can detect the time when the fault traveling wave reaches the measurement end.

The flowchart of fault traveling wave head detection based on the EFD-TEO is shown in Fig. 2. Considering the coupling effect between the three-phase lines, the current traveling wave signal is decoupled using the Karrenbauer phase mode transform. The decoupled aerial mode components are decomposed by EFD, and the decomposed high-frequency mode components are selected for TEO instantaneous energy calculation. The first energy mutation point obtained corresponds to the time when the fault traveling wave reaches the measurement end.

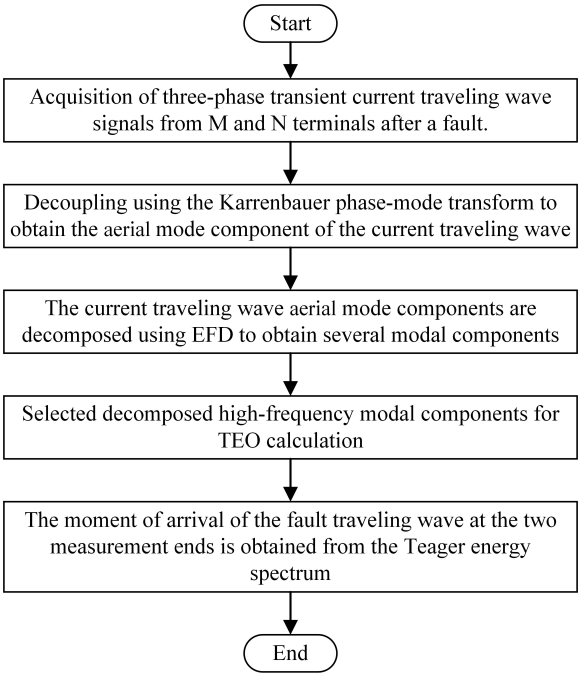

Fig. 2. Flowchart of fault traveling wave head detection based on EFD-TEO

3. Fault location method for hybrid transmission lines

3.1. Fault interval judgment

The propagation path diagram of a hybrid transmission line fault traveling wave is shown in Fig. 3. M and N are the two measuring ends of the hybrid line. F is the location of the fault, B

and D represent the connection point between the cable and the overhead line. L_1, L_2, and L_3 represent the lengths of the overhead line MB section, cable BD section, and overhead line DN section, respectively. The propagation speeds of traveling waves in the MB section, BD section, and DN section are represented by v_1, v_2, and v_3, respectively. A, C, and E represent the midpoint of the line MB, BD, and DN, respectively. D_{MF} represents the distance from the fault point F to the measurement end M. T_{M1} and T_{N1} represent the absolute time when the fault traveling wave reaches the measurement end M and N of the line, respectively [23].

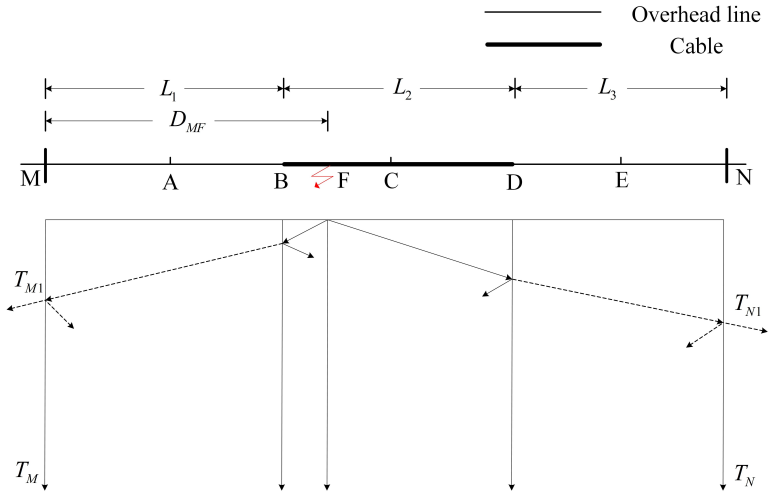

Fig. 3. Propagation path of fault traveling waves in hybrid transmission lines

When the fault occurs at A, B, C, D, E, the time difference between the fault traveling wave propagating to the two measuring terminals of the hybrid line can be defined as:

$$\begin{cases} \Delta t_1 = -\dfrac{L_2}{v_2} - \dfrac{L_3}{v_1} \\ \Delta t_2 = \dfrac{L_1}{v_1} - \dfrac{L_2}{v_2} - \dfrac{L_3}{v_1} \\ \Delta t_3 = \dfrac{L_1}{v_1} - \dfrac{L_3}{v_1} \\ \Delta t_4 = \dfrac{L_1}{v_1} + \dfrac{L_2}{v_2} - \dfrac{L_3}{v_1} \\ \Delta t_5 = \dfrac{L_1}{v_1} + \dfrac{L_2}{v_2} \end{cases}, \tag{10}$$

where Δt_1, Δt_2, Δt_3, Δt_4 and Δt_5 are the time difference between the arrival of the fault traveling wave at the two measurement ends, and these time differences correspond to faults occurring at points A, B, C, D and E, respectively.

Let the time difference between the propagation of the fault traveling wave from the fault point to the two ends is ΔT, and $\Delta T = T_M - T_N$. Where the values of T_M and T_N are obtained

by the fault traveling wave head detection method of the EFD-TEO. The size of ΔT and Δt_i $(1 \leq i \leq 5)$ is compared to determine whether the fault occurs in the first half or the second half of the line. When the fault occurs in the first half of the overhead line MB, namely the MA section, $\Delta T \leq \Delta t_1$; when the fault occurs in the second half of the overhead line MB, namely the AB section, $\Delta t_1 \leq \Delta T \leq \Delta t_2$. Within the allowable error range, when $\Delta T = \Delta t_2$, the fault can be considered to occur at or very close to the point where the overhead line and cable are connected. Similarly, when the fault occurs in the section BD of the cable line and the section DN of the overhead line, the section judgment method is consistent with the above. The judgment methods for faults occurring in different intervals are shown in Table 1.

Table 1. Judgment methods for different fault intervals

The line where the fault occurred	**Time difference comparison**	**Faulty section**
MB	$\Delta T \leq \Delta t_1$	MA
	$\Delta t_1 \leq \Delta T \leq \Delta t_2$	AB
BD	$\Delta t_2 \leq \Delta T \leq \Delta t_3$	BC
	$\Delta t_3 \leq \Delta T \leq \Delta t_4$	CD
DN	$\Delta t_4 \leq \Delta T \leq \Delta t_5$	DE
	$\Delta T \geq \Delta t_5$	EN

3.2. Fault location

After determining the half of the line segment where the fault is located, the double-ended travelling wave method is used to calculate the fault distance of that half of the line segment. Firstly, based on the time of arrival of the fault traveling wave at the measurement terminals M and N by EFD-TEO detection, combined with the time of arrival of the fault traveling wave at the measurement terminals M and N from the mid-point of each line segment and the hybrid line connection point, it is determined whether the fault occurs in the first or the second half of the line. Finally, the fault distance is calculated using the double-ended traveling wave method according to the fault section.

1. When it is determined that the fault occurred in the first half of the overhead line MB, namely the MA section, the distance x_{MF} from the fault point to the measurement end M is:

$$\begin{cases} t_{m1} = \dfrac{L_{MF}}{v_1} = T_M \\ t_{n1} = \dfrac{L_{FA}}{v_1} = T_N - \dfrac{L_1}{2 \times v_1} - \dfrac{L_2}{v_2} - \dfrac{L_3}{v_1} \\ x_{MF} = \dfrac{v_1 \times (t_{m1} - t_{n1}) + \dfrac{L_1}{2}}{2} \end{cases}, \tag{11}$$

where t_{m1} and t_{n1} are the time taken for the fault traveling wave to reach M and A from the fault point, respectively.

2. When it is determined that the fault occurs in the second half of the overhead line MB, namely the AB section, the distance x_{MF} from the fault point to the measurement end to M is:

$$\begin{cases} t_{m2} = \dfrac{L_{AF}}{v_1} = T_M - \dfrac{L_1}{2 \times v_1} \\ t_{n2} = \dfrac{L_{FB}}{v_1} = T_N - \dfrac{L_2}{v_2} - \dfrac{L_3}{v_1} \\ x_{AF} = \dfrac{v_1 \times (t_{m2} - t_{n2}) + \dfrac{L_1}{2}}{2} \\ x_{MF} = x_{AF} + \dfrac{L_1}{2} \end{cases}, \tag{12}$$

where: t_{m2} and t_{n2} are the time taken for the fault traveling wave to reach A and B from the fault point respectively, and x_{AF} is the distance from the fault point to A.

3. When the fault occurs at the connection point B of the overhead line and the cable, the distance x_{MF} from the fault point to the measuring end M is:

$$x_{MF} = L_1 \,. \tag{13}$$

Similarly, the fault location method for cable segment BD and overhead segment DN is the same as above.

3.3. Promote fault location

3.3.1. Promote fault interval judgment

A schematic diagram of a hybrid transmission line containing n ($n > 1$) sections of overhead lines and cables is shown in Fig. 4. It is assumed that the length of each section of the line is L_j, and the propagation speed of traveling waves on each section of the line is v_j, where $j = 1, 2, 3, \ldots, n$.

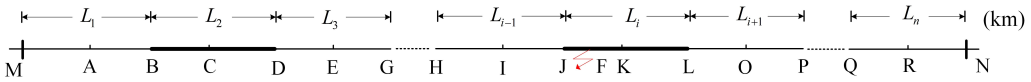

Fig. 4. Schematic diagram of n sections hybrid transmission line

1. Assuming that the fault occurs at the first end J of line i, the time difference between the arrival of the initial traveling wave of the fault at the measurement ends M and N can be expressed as:

$$\Delta t_{2i-2} = \sum_{j=1}^{i-1} \frac{L_j}{v_j} - \sum_{j=i}^{n} \frac{L_j}{v_j} \,. \tag{14}$$

2. Assuming that the fault occurs at the midpoint K of line i, the time difference between the arrival of the initial traveling wave of the fault at the measurement ends M and N can be expressed as:

$$\Delta t_{2i-1} = \sum_{j=1}^{i-1} \frac{L_j}{v_j} - \sum_{j=i+1}^{n} \frac{L_j}{v_j} \,. \tag{15}$$

3. Assuming that the fault occurs at the end L of line i, the time difference between the arrival of the initial traveling wave of the fault at the measurement ends M and N can be expressed as:

$$\Delta t_{2i} = \sum_{j=1}^{i} \frac{L_j}{v_j} - \sum_{j=i+1}^{n} \frac{L_j}{v_j}. \tag{16}$$

In the formula, $2 \le i \le n-1$, when $i = 1$, let $\sum_{j=1}^{i-1} \frac{L_j}{v_j} = 0$; when $i = n$, let $\sum_{j=i+1}^{n} \frac{L_j}{v_j} = 0$, the time difference between the initial traveling wave of the fault arriving at the measurement terminals M and N can be obtained when the fault point is in the 1st and nth segment, respectively. Therefore, the promoted fault interval judgement method can cover the whole interval. By comparing the sizes of ΔT and Δt, it is determined whether the fault occurs in the first or second half of the line. If $\Delta t_{2i-2} \le \Delta T \le \Delta t_{2i-1}$, the fault occurs in the first half of the i-th line. If $\Delta t_{2i-1} \le \Delta T \le \Delta t_{2i}$, the fault occurs in the second half of the i-th line.

3.3.2. Promote fault location

The hybrid line fault location flowchart is shown in Fig. 5. When the fault occurs in the first half of the i-th line, the distance D_{MF} from the fault point to the measuring end M can be expressed as:

$$t_{mi1} = T_m - \sum_{j=1}^{i-1} \frac{L_j}{v_j} \quad (i \ge 2), \tag{17}$$

$$t_{ni1} = T_n - \frac{L_i}{2v_i} - \sum_{j=i+1}^{n} \frac{L_j}{v_j} \quad (i+1 \le n), \tag{18}$$

$$x = \sum_{j=1}^{i-1} L_j + \frac{v_i(t_{mi1} - t_{ni1}) + \frac{L_i}{2}}{2} \quad (i \ge 2), \tag{19}$$

$$D_{MF} = \sum_{j=1}^{i-1} L_j + x \quad (i \ge 2), \tag{20}$$

where $2 \le i \le n-1$, t_{mi1} and t_{ni1} are the time taken by the fault traveling wave to reach the ends J and K, respectively, of the first half of the line i.

When the fault occurs in the second half of the i-th line, the distance D_{MF} from the fault point to the measuring end M can be expressed as:

$$t_{mi2} = T_m - \frac{L_i}{2v_i} - \sum_{j=1}^{i-1} \frac{L_j}{v_j}, \tag{21}$$

$$t_{ni2} = T_n - \sum_{j=i+1}^{n} \frac{L_j}{v_j}, \tag{22}$$

$$x = \sum_{j=1}^{i-1} L_j + \frac{L_i}{2} + \frac{v_i(t_{mi2} - t_{ni2}) + \dfrac{L_i}{2}}{2}, \tag{23}$$

$$D_{MF} = \sum_{j=1}^{i-1} L_j + \frac{L_i}{2} + x, \tag{24}$$

where: $2 \leq i \leq n-1$, t_{mi2} and t_{ni2} are the time taken by the fault traveling wave to reach the ends K and L, respectively, of the second half of the line i.

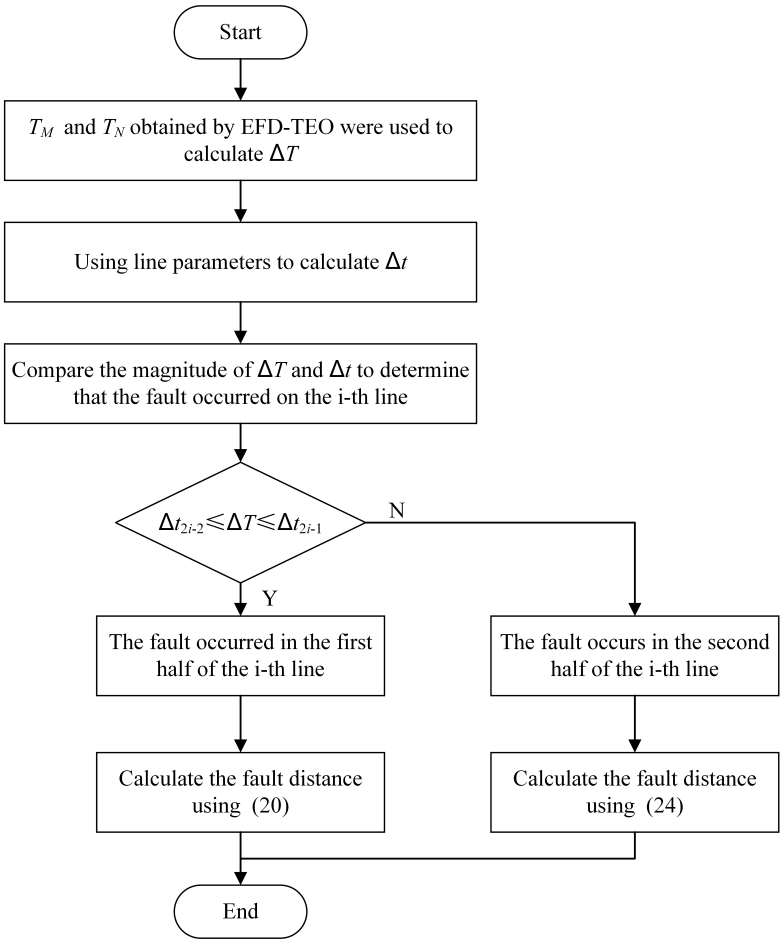

Fig. 5. Hybrid line fault location flowchart

In the above formula, when $i = 1$, let $\sum_{j=1}^{i-1} \frac{L_j}{v_j} = 0$; when $i = n$, let $\sum_{j=i+1}^{n} \frac{L_j}{v_j} = 0$. When the fault occurs in the 1st section of the line and the nth section of the line, the time at which the

initial traveling wave of the fault arrives at the ends of the half section of the line where the fault is located can be obtained respectively, and the fault distance can be calculated using the double-ended travelling wave method for this half section. Therefore, this promoted fault location method can cover the whole section.

4. Simulation analysis

4.1. Simulation model establishment

A simulation model of the 10 kV distribution network feeder system was built in PSCAD as shown in Fig. 6. The model includes three feeder lines. The third feeder is a hybrid transmission line. In this hybrid line, L_1, L_2 and L_3 denote the lengths of the MB section of the overhead line, the BD section of the cable and the DN section of the overhead line, which are 8 km, 6 km and 6 km, respectively. A, C and E denote the midpoints of the MB, BD and DN of the line, respectively. Three fault points are set as F1, F2 and F3. The distances of fault points F1, F2 and F3 from the M-terminal are 2 km, 9 km and 18 km respectively, and the simulation frequency is 1 MHz.

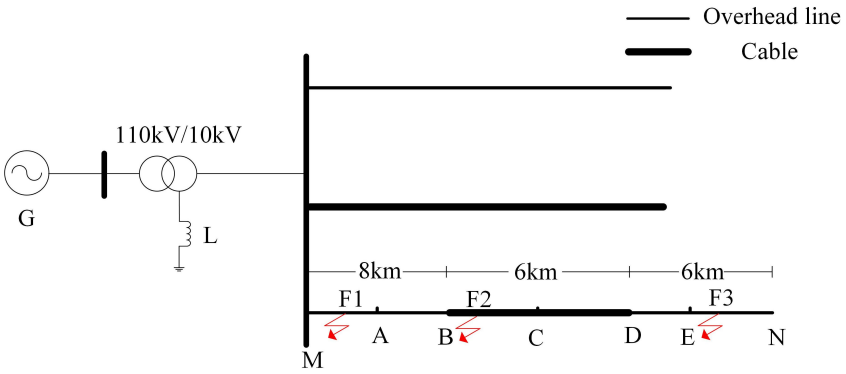

Fig. 6. 10 kV distribution network

The overhead line in the model is a frequency dependent model, and the structure of the overhead transmission line is shown in Fig. 7. In the figure, G1 and G2 represent overhead ground wires. C1, C2, and C3 represent three-phase lines A, B, and C. The conductor radius is 8.16 mm, the DC resistance is 0.0321 ohm/km, the ground wire radius is 5.52 mm, and the DC resistance is 2.8645 ohm/km. Based on the geometric parameters of the overhead line, the propagation speed of the fault traveling wave in the overhead line can be calculated as 270 km/ms.

The diagram of the geometric parameters of cable is shown in Fig. 8. The propagation speed of traveling waves in the cable line can be obtained from the geometric parameters of the cable, which is 198 km/ms. According to the line parameters, $v_1 = v_3 = 270$ km/ms, $v_2 = 198$ km/ms. According to Eq. (10), it can be calculated that $\Delta t_1 = -52.5$ µs, $\Delta t_2 = -22.9$ µs, $\Delta t_3 = 7.4$ µs, $\Delta t_4 = 37.7$ µs, $\Delta t_5 = 59.9$ µs.

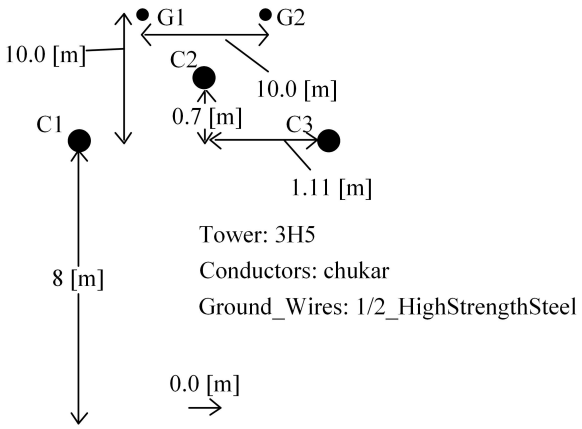

Fig. 7. Structure diagram of overhead transmission line

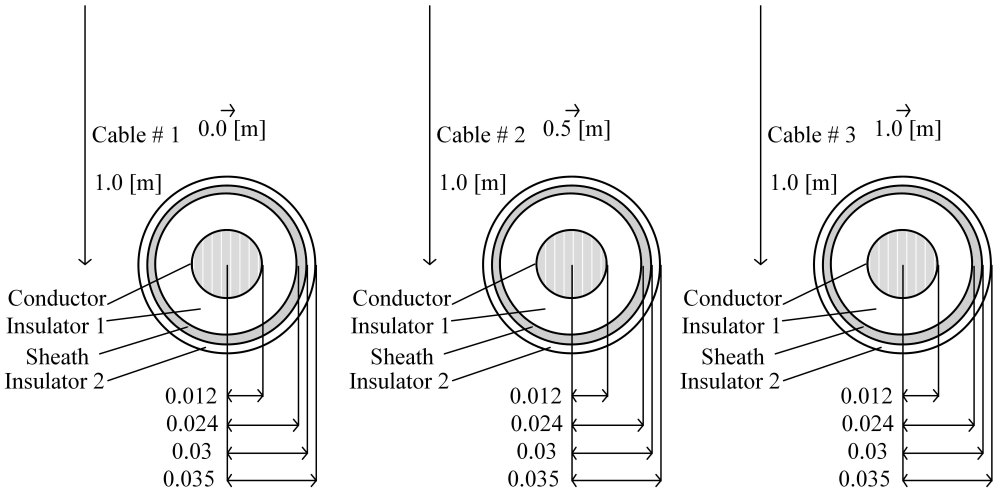

Fig. 8. Diagram of the geometric parameters of cable

4.2. Simulation results and analysis

4.2.1. Different fault distance

A single-phase ground fault is set up at F2, the fault occurrence moment is 2 ms, the fault duration is 0.05 s, the sampling frequency of the processing signal is 1 MHz, the grounding resistance is 0.01 Ω, and the current traveling wave aerial mode component from 1 ms to 3 ms is analysed. The distance from the fault point F2 to the hybrid line connection B is 1 km and the distance to the measurement end M is 9 km. The number of modal decompositions of EFD is set to 3. In this paper, we use EFD to decompose the current transient travelling wave modal components into three modal components, and select the third high-frequency modal component for the TEO

operation, to obtain the fault travelling wave arrival moment. The fault feature extraction process of current aerial mode components at F2 through the EFD-TEO is shown in Fig. 9.

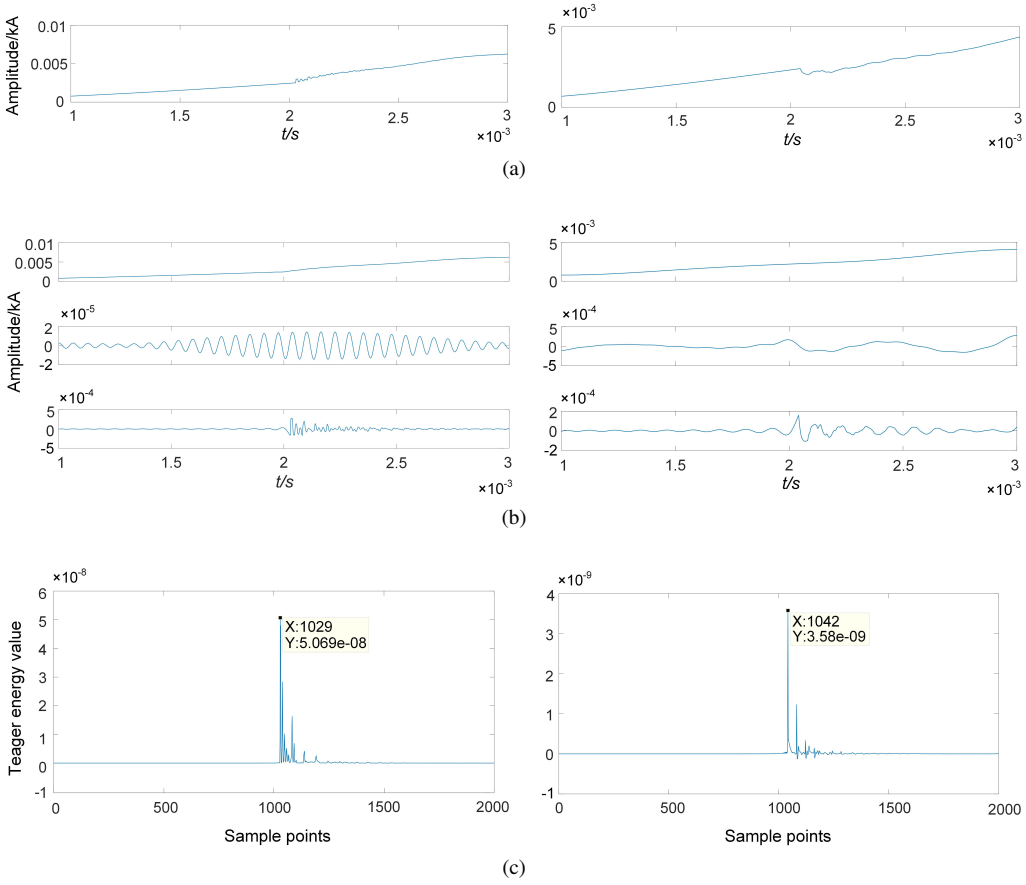

Fig. 9. Fault feature extraction process of current aerial mode components at F2 through EFD-TEO: (a) aerial mode component of current at M and N terminals during F2 fault; (b) EFD decomposition results of the aerial mode components of the M and N terminal currents during F2 fault; (c) Teager energy spectrum of mode 3 obtained from M and N terminals during F2 fault

From the energy mutation point in the Teager energy spectrum, it can be seen that the time when the initial traveling wave of the fault reaches the M end and N end is $T_M = 29$ μs and $T_N = 42$ μs, respectively. It can be calculated that $\Delta T = T_M - T_N = -13$ μs. By comparing $\Delta t_2 \leq \Delta T \leq \Delta t_3$, it can be determined that the fault zone is in the BC section, which is the first half of cable line L_2. Substituting T_M and T_N into Eqs. (17) and (18) respectively, it can be obtained that $X_{BF} = 0.9797$ km, the distance from the measurement end M is $X_{AF} = L_1 + X_{BF} = 8.9797$ km, and the ranging error is 20.3 m. The location results when the fault is occurred at F1, F2 and F3 under the same fault conditions are shown in Table 2.

Table 2. Localization results under different fault distances

Fault distances / km	T_M	T_N	Fault section	Location results / km	Errors / m
2	1 005	1 072	MA	2.0459	45.9
9	1 029	1 042	BC	8.9797	20.3
18	1 073	1 005	EN	18.0891	89.1

4.2.2. Different transition resistances

As the amplitude of the traveling wave decreases with the increase in the transition resistance, which in turn affects the accuracy of the travelling wavehead detection, it also has an impact on the fault location results. In this paper, the transition resistors of 0.01 Ω, 20 Ω and 400 Ω are respectively set to verify the influence of the proposed method on fault location accuracy. On the hybrid line, the distance from the fault point to the M-terminal is set to 2 km and 18 km. The transition resistance is set to 0.01 Ω, and the fault type is single-phase ground fault, and the data before and after the fault is taken for 1ms to be analysed, and the fault location results are shown in Table 3.

Table 3. Positioning results under different transition resistances

Fault distances / km	Fault resistances / Ω	T_M	T_N	Fault section	Location results / km	Errors / m
2	0.01	1 005	1 072	MA	2.0459	45.9
	20	1 005	1 072	MA	2.0459	45.9
	400	1 005	1 072	MA	2.0459	45.9
18	0.01	1 073	1 005	EN	18.0891	89.1
	20	1 073	1 005	EN	18.0891	89.1
	400	1 073	1 005	EN	18.0891	89.1

4.2.3. Different fault types

In order to verify the effect of different fault types on the proposed method, single-phase ground faults (Ag), two-phase ground faults (ABg) and interphase faults (AB) are set up in this paper to verify the effect of the proposed method on the fault location accuracy. On the hybrid line L_c, the distances from the fault point to the M end are set to 9 km and 18 km. The transition resistance is set to be 0.01 Ω, and the data before and after the fault are taken for 1ms to be analysed. The fault location results are shown in Table 4.

From the positioning results in the above tables, it can be seen that under different fault conditions, the fault location method proposed in this paper can accurately identify the fault section and has high location accuracy, and the fault location results are less affected by the transition resistance and fault type, which verifies that this method has high location accuracy and good reliability.

Table 4. Localization results under different fault types

Fault distances / km	Fault resistances / Ω	T_M	T_N	Fault section	Location results / km	Errors / m
9	Ag	1 029	1 042	BC	8.9797	20.3
	ABg	1 028	1 041	BC	8.9797	20.3
	AB	1 029	1 042	BC	8.9797	20.3
18	Ag	1 073	1 005	EN	18.0891	89.1
	ABg	1 073	1 005	EN	18.0891	89.1
	AB	1 073	1 005	EN	18.0891	89.1

4.3. Comparison of positioning results of different wave head detection methods

The EMD-TEO method and the variational mode decomposition (VMD)-TEO method are used to compare with the method of this paper, a single-phase ground fault is set up at 10 km from the measurement end of M, the fault occurrence moment is 2 ms, the fault duration is 0.05 s, and the grounding resistance is 0.01 Ω, and the current traveling wave aerial mode components before and after the fault of 1ms are analysed. The EMD-TEO method uses EMD to decompose the current aerial mode component and selects the first modal component for TEO analysis; the penalty factor in VMD is set to 1 200, and the number of decomposed modes K is set to 4. The aerial mode component of the above fault is decomposed by VMD, and the second modal component is selected for TEO analysis. The energy mutation point in the Teager energy spectrum is the moment when the initial traveling wave of the fault reaches the measurement end. The aerial mode component of this fault is processed by the VMD-TEO as shown in Fig. 10. With the above

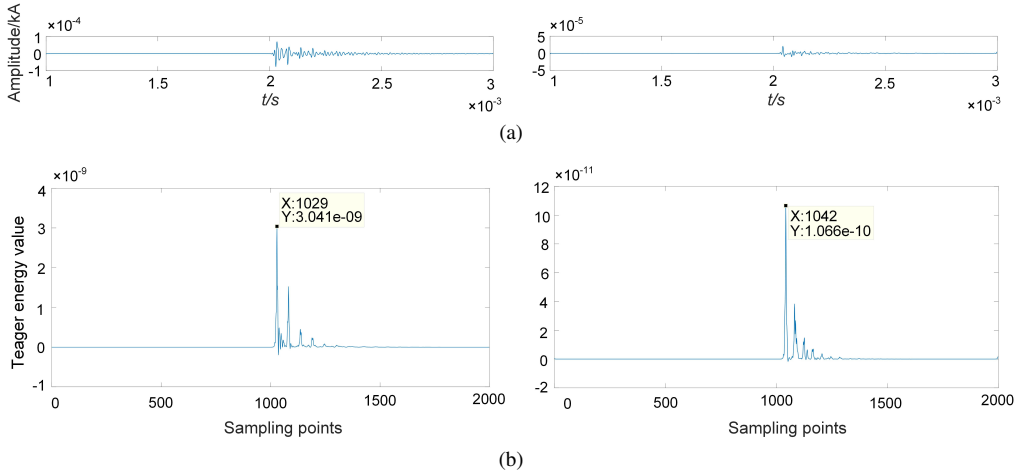

Fig. 10. Fault feature extraction process of current aerial mode component at 9 km through VMD-TEO: (a) VMD decomposition results of the current aerial mode components at the M and N terminals at F2; (b) Teager energy spectrum of the second modal component obtained from the M and N terminals during the F2 fault

fault conditions unchanged, the fault distance is changed and the location results by the VMD-TEO and EMD-TEO at different fault distances are shown in Table 5.

Table 5. Localization results of different wave head detection methods

Method	Fault distances / km	T_M	T_N	Fault section	Location results / km	Errors / m	Average accuracy
EMD-TEO	2	1 004	1 070	MA	2.1809	180.9	96.94%
	5	1 012	1 056	AB	5.1509	150.9	
	8	1 022	1 046	AB	7.8509	149.1	
	9	1 031	1 043	BC	9.0787	78.7	
	18	1 074	1 006	EN	18.0891	89.1	
VMD-TEO	2	1 005	1 073	MA	1.9109	89.1	98.31%
	5	1 013	1 059	AB	4.8809	119.1	
	8	1 024	1 046	BC	8.0887	88.7	
	9	1 029	1 042	BC	8.9797	20.3	
	18	1 073	1 006	EN	17.9541	45.9	
EFD-TEO	2	1 005	1 072	MA	2.0459	45.9	98.88%
	5	1 013	1 059	AB	4.8809	119.1	
	8	1 024	1 047	AB	7.9859	14.1	
	9	1 029	1 042	BC	8.9797	20.3	
	18	1 073	1 005	EN	18.0891	89.1	

From Table 5, it can be seen that the location error of the EFD-TEO method proposed in this paper is lower than that of the EMD-TEO method and the VMD-TEO. Therefore, the method proposed in this paper has a higher location accuracy compared to other fault location methods.

4.4. Comparison of computational efficiency of different signal decomposition methods

When a single-phase ground fault occurs at F1, F2 and F3 of the hybrid line, the current traveling wave aerial mode component data collected at the M-terminal are denoted by f_1, f_2, f_3, respectively, and the transition resistance at the time of the fault is 0.01 Ω. The EMD, VMD and EFD methods are used to decompose f_1, f_2, f_3, respectively, and then their computational efficiencies are compared. The calculation was conducted on MATLAB R2017a, with Intel (R) Core (TM) i5-8250U CPU, 8.0 GB RAM, and 64 bit Windows 11 on the PC. The computational efficiency of different signal decomposition methods is shown in Table 6.

From Table 6, it can be seen that for the same fault signal, the computational efficiency of EFD is higher than that of EMD and VMD. Therefore, the proposed method in this paper has a better performance in fault location accuracy and computational efficiency, which is conducive to fast and accurate fault location.

Table 6. Calculation efficiency of different signal decomposition methods

Signal	Computation time (s)		
	EMD	VMD	EFD
f_1	0.433809	0.394003	0.317821
f_2	0.433718	0.407193	0.388358
f_3	0.418520	0.425266	0.327436

5. Conclusions

In this paper, a double-ended traveling wave fault localisation method based on the EFD-TEO is proposed, and the following conclusions are drawn through extensive simulations in PSCAD and MATLAB.

1. In this paper, the fault location method proposed in this paper is compared with the EMD-TEO and VMD-TEO in terms of fault location accuracy and decomposition efficiency of fault signals, and it is verified that the method proposed in this paper has better performance in terms of fault location accuracy and computational efficiency.
2. A method for judging the fault section of a hybrid line based on the midpoint of each section and the connection point of the hybrid line is proposed. By determining whether the fault occurs in the first half or the second half of the line, it is possible to more accurately determine the fault section of the hybrid line.
3. A 10 kV small-current grounding system model containing hybrid lines was built on PSCAD. The simulation was carried out by setting different transition resistances, fault distances and fault types. And a large amount of simulation data was analysed in MATLAB using the travelling wave location method of the EFD-TEO. Thus, it is verified that the fault location method proposed in this paper has high location accuracy, computational efficiency and good reliability for hybrid lines, which is more conducive to the fast and accurate location of the fault point.

References

[1] Daisy M., Dashti R., *Single phase fault location in electrical distribution feeder using hybrid method*, Energy, vol. 103, pp. 356–368 (2016), DOI: 10.1016/j.energy.2016.02.097.

[2] Shu H., Liu X., Tian X., *Single-Ended Fault Location for Hybrid Feeders Based on Characteristic Distribution of Traveling Wave Along a Line*, IEEE Transactions on Power Delivery, vol. 36, no. 1, pp. 339–350 (2021), DOI: 10.1109/TPWRD.2020.2976691.

[3] Guruajapathy S.S., Mokhlis H., Illias H.A., *Fault location and detection techniques in power distribution systems with distributed generation: A review*, Renewable and Sustainable Energy Reviews, vol. 74, pp. 949–958 (2017), DOI: 10.1016/j.rser.2017.03.021.

[4] Wang X., Gao J., Wei X., Zeng Z., Wei Y., Kheshti M., *Single line to ground fault detection in a non-effectively grounded distribution network*, IEEE Transactions on Power Delivery, vol. 33, no. 6, pp. 3173–3186 (2018), DOI: 10.1109/TPWRD.2018.2873017.

[5] Lee Y.J., Lin T.C., Liu C.W., *Multi-Terminal Nonhomogeneous Transmission Line Fault Location Utilizing Synchronized Data*, IEEE Transactions on Power Delivery, vol. 34, no. 3, pp. 1030–1038 (2019), DOI: 10.1109/TPWRD.2018.2890337.

[6] Li X., Liu S., Huang R., Ai J., An Y., Chen P., Xin Z., *Study on accuracy traveling wave fault location method of overhead line — Cable hybrid line and its influencing factors*, 2017 Chinese Automation Congress (CAC), Jinan, China, pp. 4593–4597 (2017), DOI: 10.1109/CAC.2017.8243590.

[7] Lin T.C., Lin P.Y., Liu C.W., *An algorithm for locating faults in three-terminal multisection nonhomogeneous transmission lines using synchro phasor measurements*, IEEE Transactions on Smart Grid, vol. 5, no. 1, pp. 38–50 (2014), DOI: 10.1109/TSG.2013.2286292.

[8] Wang L., Liu H., Dai L.V., Liu Y., *Novel Method for Identifying Fault Location of Mixed Lines*, Energies, vol. 11, no. 6, 1529 (2018), DOI: 10.3390/en11061529.

[9] Tian S., Yang Q., Xu Y., Zhang T., *Accurate fault location of hybrid lines in distribution networks*, International Transactions on Electrical Energy Systems, vol. 31, no. 12, e13158 (2021), DOI: 10.1002/2050-7038.13158.

[10] Reis R.L.A., Lopes F.V., *Correlation-based single-ended traveling wave fault location methods: A key settings parametric sensitivity analysis*, Electric Power Systems Research, vol. 213, 108363 (2022), DOI: 10.1016/j.epsr.2022.108363.

[11] Lopes F.V., Lima P., Ribeiro J.P.G., *Practical methodology for two-terminal traveling wave-based fault location eliminating the need for line parameters and time synchronization*, IEEE Transactions on Power Delivery, vol. 34, no. 6, pp. 2123–2134 (2019), DOI: 10.1109/TPWRD.2019.2891538.

[12] Lopes F.V., Dantas K.M., Silva K.M., Costa F.B., *Accurate two-terminal transmission line fault location using traveling waves*, IEEE Transactions on Power Delivery, vol. 33, no. 2, pp. 873–880 (2018), DOI: 10.1109/TPWRD.2017.2711262.

[13] Liang R., Wang F., Fu G., Xue X., Zhou R., *A general fault location method in complex power grid based on wide-area traveling wave data acquisition*, International Journal of Electrical Power & Energy Systems, vol. 83, pp. 213–218 (2016), DOI: 10.1016/j.ijepes.2016.04.021.

[14] Naidu O.D., Pradhan A.K., *Precise Traveling Wave-Based Transmission Line Fault Location Method Using Single-Ended Data*, IEEE Transactions on Industrial Informatics, vol. 17, no. 8, pp. 5197–5207 (2021), DOI: 10.1109/TII.2020.3027584.

[15] Xie L., Luo L., Ma J., Li Y., Zhang M., Zeng X., Cao Y., *A novel fault location method for hybrid lines based on traveling wave*, International Journal of Electrical Power & Energy Systems, vol. 141, 108102 (2022), DOI: 10.1016/j.ijepes.2022.108102.

[16] Duan J., *Single Terminal Traveling Wave Method for Hybrid Line Ground Fault Location Based on EEMD and SDEO*, 2019 IEEE 8th International Conference on Advanced Power System Automation and Protection (APAP), Xi'an, China, pp. 815–819 (2019), DOI: 10.1109/APAP47170.2019.9225068.

[17] Gashteroodkhani O.A., Majidi M., Etezadi-Amoli M., Nematollahi A.F., Vahidi B., *A hybrid SVM-TT transform-based method for fault location in hybrid transmission lines with underground cables*, Electric Power Systems Research, vol. 170, pp. 205–214 (2019), DOI: 10.1016/j.epsr.2019.01.023.

[18] Xu Y., Zhao C., Xie S., Lu M., *Novel Fault Location for High Permeability Active Distribution Networks Based on Improved VMD and S-transform*, in IEEE Access, vol. 9, pp. 17662–17671 (2021), DOI: 10.1109/ACCESS.2021.3052349.

[19] Zhou W., Feng Z., Xu Y.F., Wang X., Lv H., *Empirical Fourier decomposition: An accurate signal decomposition method for nonlinear and non-stationary time series analysis*, Mechanical Systems and Signal Processing, vol. 163, 108155 (2022), DOI: 10.1016/J.YMSSP.2021.108155.

[20] Singh P., Joshi S.D., Patney R.K., Saha K., *The Fourier decomposition method for nonlinear and non-stationary time series analysis*, Proceedings of the Royal Society A, Mathematical, physical, and engineering sciences, vol. 473, no. 2199 (2017), DOI: 10.1098/rspa.2016.0871.

[21] Gilles J., *Empirical Wavelet Transform*, IEEE Transactions on Signal Processing, vol. 61, no. 16, pp. 3999–4010 (2013), DOI: 10.1109/TSP.2013.2265222.

[22] Tran V.T., Althobiani F., Ball A., *An approach to fault diagnosis of reciprocating compressor valves using Teager-Kaiser energy operator and deep belief networks*, Expert Systems with Applications, vol. 41, no. 9, pp. 4113–4122 (2014), DOI: 10.1016/j.eswa.2013.12.026.

[23] Naidu O.D., Pradhan A.K., *A Traveling Wave-Based Fault Location Method Using Unsynchronized Current Measurements*, in IEEE Transactions on Power Delivery, vol. 34, no. 2, pp. 505–513 (2019), DOI: 10.1109/TPWRD.2018.2875598.